ASME Open Journal of Engineering
Online journal at:
https://asmedigitalcollection.asme.org/openengineering

Experimental Validation of Analytical Predictions for the "Deviant" Density of Oleo-Nanofluids Based on the nanoFin Effect

Ritwik Bhattacharya
Department of Mechanical Engineering,
Texas A&M University,
3123 TAMU,
College Station, TX 77843
e-mail: rbhattachar8@tamu.edu

Jonghyun Lee
Department of Mechanical Engineering,
Texas A&M University,
3123 TAMU,
College Station, TX 77843
e-mail: jlee0501@tamu.edu

Anindito Sen
Microscopy and Imaging Center (MIC),
Texas A&M University,
3123 TAMU,
College Station, TX 77843
e-mail: andysen@tamu.edu

Debjyoti Banerjee[1]
Professor
J. Mike Walker '66 Department of Mechanical Engineering,
Texas A&M University,
3123 TAMU,
College Station, TX 77843
e-mail: dbanerjee@tamu.edu

Experimental validation of the analytical predictions for the "deviant" density enhancement of nanofluids is presented in this study. Experimental measurements of density were complemented by transmission electron microscopy (TEM) of these nanofluid samples. The analytical model predicts the effective density of the nanofluid as a function of the mass fractions and densities of the nanoparticle, the base solvent, and the "compressed phase" of the solvent encapsulating the nanoparticle. In this study, casein is used as the nanoparticle candidate at a mass fraction of 1% and paraffin oil (which is essentially a phase change material (PCM)) is used as the neat solvent (base fluid). The experimental measurements demonstrate anomalous enhancement of the density of the oleo-nanofluids, which is 7% in excess of the value predicted by the conventional mixing rule (with a measurement uncertainty less than 1.2%). The formation of a compressed phase within the nanofluid domain is responsible for the "surplus" density (deviant density) of the oleo-nanofluid. The predicted values are found to closely match the actual dimensions of the nanostructures measured in the TEM images, hence conclusively validating the numerical model for estimating the magnitude of the deviant density contributed by the compressed phase. This also confirms the presence of a compressed phase (which is a consequence of the "nanoFin effect"), that was investigated and validated in this study. This surplus densification in hydrocarbons (such as PCM and oil-based nanofluids) makes them potentially attractive candidates as radiation shielding materials (e.g., for deep space exploration applications).
[DOI: 10.1115/1.4065511]

Keywords: advanced energy systems simulation, advanced manufacturing, advanced materials and processing simulation, advanced materials characterization, aerospace heat transfer, aerospace systems, experimental heat transfer, experimental research for nuclear safety, experimental techniques, experimental/measurement techniques, experimentation in fluid mechanics and energetic, extended surfaces, extended surfaces/fins, flows in biological systems, flows in porous media, fluid control systems, fluid flow, fluid mechanics/dynamics, fluidics, heat and mass transfer, heat and mass transfer simulation, heat energy generation/storage/transfer, heat transfer and film cooling, heat transfer augmentation techniques, heat transfer enhancement, hierarchical modeling, liquid–solid, low temperature heat transfer, micro and nano systems design and synthesis of, micro/nanoscale heat transfer, microfluidics, microfluidics and nanofluidics, microscale fluid flow and heat and mass transfer, microstructural size effect, microstructure, microstructure effect, microstructure property relationships, microsystems, microtechnology, microtexture, miniaturization, minimally invasive devices, mixed convection, multi-scale modeling, multiphase flow, multiphase flow characterization and analysis, multiphase flows, multiphysics modeling and simulation, multi-scale modeling and simulation, nano devices, nano surface engineering, nano systems, nanoscale flows, nanofluids, nanofluids heat transfer, nanomanufacturing, nanomaterials, nanomechanics, nanoscale heat transfer, nanostructure, nanostructure (quantum dot, nanowire), nanotechnolgy, nanotechnology, nanotribology, Newtonian

[1]Corresponding author.
Manuscript received April 17, 2024; final manuscript received May 6, 2024; published online May 30, 2024. Assoc. Editor: Hameed Metghalchi.

flows, non-Fourier heat conduction, non-newtonian flows, nuclear safety and security, numerical modeling of heat transfer and fluid flow, optimization algorithms, optimization and control, optimization and design sensitivity analysis of non-linear systems, petroleum, petroleum engineering, petroleum engineering simulation, petroleum transport/pipelines/multiphase flow, pharmaceuticals, phase change materials, phase transitions, phase change and convective heat transfer, physical fluid dynamics, process engineering, process modeling for engineering applications, processing and manufacturing, protein kinematics, quantum dots, radiation, radiation science and radiation protection, radiative heat transfer, renewable energy, rheology, solar energy, solar energy and applications, solar reactor, solar receiver, solar thermal, solar thermal power, space, spacecraft control, sports instrumentation and devices, thermal, thermal analysis, thermal and energy systems/devices with boilers and condensers, thermal characterization, thermal comfort, thermal energy storage, thermal engineering of power plant, thermal hydraulics, thermal insulation, thermal management, thermal management of batteries, thermal management of electronics, thermal power, thermal radiation, thermal systems, thermal technique, thermal hydraulics, thermal hydraulics nuclear reactor safety, thermally assisted micro-manufacturing, thermocouples, thermodynamics, two-phase flow, two-phase flow and heat transfer, ultrasonics, uncertainty analysis, uncertainty characterization, uncertainty modeling, uncertainty quantification

1 Introduction

Nanoparticles can be defined as microscopic particles with at least one dimension measuring less than 100 nm. The term "nanofluid" refers to stable colloidal suspensions of nanoparticles within a particular solvent. Anomalous variations in the material properties of nanofluids (e.g., non-Newtonian rheological properties, density, thermal conductivity, and specific heat capacity), in comparison with that of the neat solvent, have led to many conflicting studies in the contemporary literature in the past couple of decades. The nanofluid literature is replete with controversial and conflicting reports and discussions on the anomalous variation of material properties of nanofluids as compared to those of base solvents (such as water, glycols, oil, and molten salts) [1–3].

The field of nanofluid research is abundant with contradictory findings and disputes, stemming from the varying observations of improvements (or deteriorations) in the material properties of these nanofluids, as documented by diverse groups of researchers. The source of these disputes can be traced to their roots in (a) deficiency of proper due diligence or lack of attention to properly documenting the synthesis protocols, and (b) also includes insufficient design of experiments [4]. Furthermore, the material characteristics of nanofluids frequently exhibit strong susceptibility to slight deviations in the synthesis protocols. This susceptibility arises because the stability of the nanofluids is profoundly influenced by a wide range of parameters (including those of the synthesis procedures). For instance, during batch fabrication, it is crucial to meticulously plan and strictly follow precisely the properly regimented steps of the synthesis protocols of the nanofluid samples. This requires attention to detail, precise calibration of the measurement procedures, and close monitoring of the various process parameters. As a result of the laxity in due diligence, the early literature reports frequently failed to strictly regulate the synthesis procedure, including the verification of nanoparticle size and shape (as well as their long-term stability in colloidal suspensions). These studies also lacked the implementation of proper control experiments, both prior to and following each experimental trial [4].

Although stable colloidal nanoparticle suspensions in solvents can be misconstrued as a two-phase mixture, the unusual variations in material properties of these nanofluids can be ascribed to the formation of a "third phase" within the bulk solvent, which surrounds individual nanoparticles (and can result in the formation of a percolation network that emanates from this third phase). There is a rearrangement of the molecules of the solvent phase at the surface of the nanoparticle due to the adsorption of the solvent molecules on the nanoparticle surface. This rearranged phase can even imitate the crystalline structure of the solid surface beneath it [5]. The existence of the third phase (referred to as the "compressed phase") was confirmed by multiple researchers through techniques, such as molecular dynamics (MD) simulations, as well as experimental methods including electron microscopy and X-ray diffraction analysis [2,6]. The compressed stage exhibits greater density and usually possesses a thickness that typically falls within the range of 1–2 nm. These literature accounts also revealed the extent of density fluctuations within the compressed phase. Frequently, the exponentially decreasing peak densities in the density profile seemed to be spreading away from the surface of the nanoparticles [7].

Additional investigation is required into the coupled non-linear transport mechanisms that give rise to these unusual variations in material properties. The existing models in scientific literature frequently fall short of comprehensively depicting the complete range of deviant patterns shown by all types of nanofluids. For instance, aqueous nanofluids exhibit reduced specific heat capacity values; whereas non-aqueous nanofluids (e.g., molten salt nanofluids) and oleo-nanofluids display increased specific heat capacity values compared to that of the base solvent. These unusual behavioral trends can be attributed to the buildup of the compressed phase that surrounds the nanoparticles [8]. Advanced research has revealed the emergence of secondary nanostructures originating from the compressed phase. This leads to the creation of a percolation network composed of a semi-crystalline phase that penetrates through the bulk (amorphous) solvent phase, akin to cobwebs [9,10]. Nanofluid samples in which the secondary nanostructure was absent did not display any enhancement in specific heat capacity values. Advanced numerical models are currently being developed to accurately forecast the increase in specific heat capacity in these nanofluid samples [11]. Formation of this compressed phase due to surface adsorption of the solvent molecules on the surface of the nanoparticle can therefore be implied to cause the "nanoFin effect" (nFE), which is described next.

1.1 nanoFin Effect.

The nFE can adequately explain and model the compressed phase formation which gives rise to unusual deviations in the material properties of nanofluids [12]. An instance of the nanoFin effect becomes apparent when nanoparticle coatings formed by nanoparticles induce "anomalous" thermal performance. In the course of phase-change phenomena such as boiling on nanostructured heaters, for example, it has been observed that nanofins formed from nanoparticles (as coatings) that have lower magnitudes of thermal conductivity can result in greater enhancements in heat flux values, in contrast to nanoparticles with higher thermal conductivity values [12].

Previous experimental studies on pool boiling conducted on nanostructured heater surfaces have shown that heater surfaces coated with nanofins of lower thermal conductivity show a higher level of enhancement in critical heat flux (CHF) compared to surfaces coated with nanofins of higher thermal conductivity. As an example, when considering silicon heater surfaces featuring etched silicon nanofins, there was a 120% improvement in CHF compared to the 60% enhancement observed in silicon substrates coated with carbon nanotubes (CNT) [13]. These unusual experimental findings can be explained by the interfacial thermal resistance, referred to as the "Kapitza resistance" [14–16] existing between the surface of the nanofin and the surrounding solvent molecules. This resistance arises due to the mismatch in the transmission of thermo-mechanical vibrations between the nanofin surface and the solvent molecules [17]. Therefore, the significant improvement in heat transfer enhancement with silicon nanofins can be attributed to their markedly reduced interfacial resistance, which is three orders of magnitude lower compared to CNT-coated heaters [18–20]. Hence, due to the reduced effective thermal resistance in silicon nanofins compared to CNTs, which includes the Kapitza resistance, there is an overall increase in heat flux enhancement levels for silicon nanofins. As a result, the Kapitza resistance holds the primary role within the thermal impedance network of these nanofins, constituting the major portion of the overall thermal resistance [7,21,22]. Jo [7] used MD simulations to explore the consequences arising from the buildup of a compressed phase of solvent molecules surrounding different nanoparticles (such as single-walled carbon nanotube (SWCNT), graphite sheets, and C_{60} fullerene) within a high-temperature molten salt eutectic. These simulations showed that the thickness of the compressed layer surrounding the nanoparticle displayed minimal sensitivity to the nanoparticle's size or shape when considering a specific combination of solid and fluid (solvent) materials.

Furthermore, the thermophysical properties of the nanoparticle mixture were demonstrated to be influenced by the spatial variation of concentration, arising from factors like Van der Waals forces and ionic interactions within the solvent and near the nanofins. The findings signaled the presence of oscillations in the density and ionic concentration profiles within the solvent phase. These fluctuations in oscillations would result in significant changes in the concentration gradients of different species (with varying rates of attenuation of species concentration values for each species, moving away from the nanoparticle surface). Classical force field models were applied in MD simulations to obtain these estimates [7]. The MD simulations also demonstrated that the compressed phase has a thickness ranging from 1 nm to 2 nm [7], with a "void space" between the solvent molecules and the surface of the nanoparticle. The void space thickness on the surface of the nanoparticle (devoid of any solvent molecules) is estimated to be ~5 Å (~0.5 nm). This void space is essentially the average equilibrium intermolecular spacing between the solvent molecules and the atoms on the nanoparticle surface. Yang [23] examined the effects of the compressed layer on the transient heat transfer in nanoparticle suspensions, as well as its impact on heaters with nanostructured surfaces. The surface adsorption of the fluid molecules on the solid surfaces causes local changes in the thermal characteristics as a result of variations in the values of the thermal properties of the bulk phase and the compressed phase. The study involved observing the density profile in the vicinity of a SiO_2 nanoparticle that was surrounded by a refrigerant (PF5060, the chosen working fluid for the pool boiling experiments in this study [23]). In line with previous findings in the literature [24,25], Yang's study [23] revealed that the thickness of the compressed layer was around 1 nm. Additionally, the anticipated peak density of the compressed phase aligned with the solid phase density of the solvent, corresponding to roughly double the values observed in the bulk phase. Moreover, it was found that the primary mechanism behind the improvement in the effective specific heat capacity of nanocomposites (such as nanoparticles dispersed within a solvent) is the buildup of a compressed phase of the solvent molecules encircling the nanoparticles or nanofins [26]. The compressed phase formation resulting from the adsorption on the surface and the subsequent rearrangement of solvent molecules on the nanoparticle (or nanofin) can serve as an additional transport mechanism for enhanced thermal energy storage.

In addition, nFE implies that along with the density fluctuations of the solvent molecules on the nanoparticle surface—the transport mechanisms can be severely influenced by strong concentration gradient values arising from associated oscillations in species concentration. The buildup of a concentration gradient of the solvent molecules on the surface of the nanoparticle, i.e., nanofin, gives rise to a bias that regulates the heat flux based upon the directionality of the temperature difference, hence mimicking the behavior of a thermal "diode." In other words, the nFE model predicts the formation of a thermal diode on the surface of the nanoparticle (or nanofin) [23]. The thermal diode-like phenomenon occurs due to mass transfer (or diffusion) driven by the gradient in chemical concentration. This leads to a situation where a higher heat flux is attained when a hot nanoparticle is in contact with a colder solvent phase. In this scenario, the thermal gradient and species concentration gradients are aligned, meaning they decrease in the same direction. Conversely, when a cold nanoparticle is in a hot solvent phase, the thermal gradient and species concentration gradients oppose each other, as they decrease in opposite directions. Consequently, for a similar temperature difference between two nanoparticles and the liquid phase, a nanofin having a higher temperature than the liquid phase is likely to exhibit 2–10% higher heat flux as compared to a nanofin having a lower temperature (for a given combination of materials selected for these experimental studies).

To put it briefly, the introduction of nanoparticles in a base solvent (or the modification of the surface of heaters by fabricating nanostructures or nanofins) frequently leads to unusual deviations in material properties such as thermal conductivity and specific heat capacity. This can also enhance the magnitudes of heat flux, especially leading to the enhancement of phase-change heat transfer (e.g., boiling) [12]. The non-linear coupling of the transport mechanisms associated with the gradients in temperature and mass concentration profiles is primarily responsible for the nFE. An amalgamation of transportation mechanisms was suggested by Singh and Banerjee [12], primarily influenced by three separate mechanisms, and they have been outlined as follows:

(1) Solvent molecules get adsorbed on the surface of the nanoparticle and form a compressed phase, which is a nanoscale layer on the solid surface having an average thickness of 1–2 nm. This "third phase" possesses different values of effective mass density and specific heat capacity compared to the bulk solvent phase and consequently influences the overall thermal resistance and thermal capacitance of the mixture.
(2) The impedance mismatch in the thermal-transport-induced molecular and atomic scale vibrations between the solvent molecules and the atoms on the nanoparticle surface results in the generation of an interfacial thermal resistance between the nanoparticle and solvent molecule (known as "Kapitza resistance").
(3) Mass diffusion occurs due to concentration gradients that arise from the selective adsorption of various solvent species onto nanoparticle surfaces. This adhesion of solvent species to nanoparticles leads to variations in both mass concentration and ionic concentration gradients among the solvent species. Consequently, these variations play a role in the creation of a phenomenon similar to a "thermal diode."

The manifestation of nFE is acute in the following cases [12]: (i) when the diameters of the nanoparticles are less than 10 nm (it is even better when the nanoparticle diameter is less than 6 nm); (ii) when the density of the nanoparticle is less than 1 g/cc; (iii) when the solid phase density of the solvent is higher than its liquid phase density; (iv) when the liquid phase density of the solvent is lower than 1 g/cc; (v) when the solid phase density of the solvent

is more than 1 g/cc; (vi) when the ratio of the solid phase density to the liquid phase density of the solvent is less than 1; and (vii) when the nanofluid involves the combination of nanoparticle and base solvent in a way so that the thickness of the compressed phase is maximized via various means, like the control of pH or Zeta potential (for fluids which are ionic in nature) or changing the concentration of surfactant (for polar fluids). This demonstrates that detecting the effects of nFE is extremely challenging (almost negligible) in the case of aqueous nanofluids while being more noticeable in non-aqueous solvents (such as oleo-nanofluids, molten salt nanofluids, etc.).

In contrast to the abundance of literature discussing the thermal conductivity of nanofluids (and to a lesser degree, literature covering the specific heat capacity of nanofluids), our literature review has identified only a handful of reports that have sincerely undertaken experimental measurements for nanofluid density values, even though some inaccuracies were noted. Out of the experimental measurements documented in various literature reports, only six [27–32] have explored the reasons behind variations in density values of nanofluids. These variations were attributed to the creation of a compacted layer, occasionally denoted as the "nanolayer" in these literature accounts. Notably, one study [27] assumed that the simple mixing rule holds true and went on to propose a correction factor, despite the surplus density surpassing 8% in certain instances among the nanofluid samples they utilized in their experimental assessments.

Most of the studies documented in the literature employed classical or simple mixing model for the estimating density of nanofluids. They utilized a linear approach for predicting density values and volume fractions based on thermodynamic equilibrium. As previously noted, only a limited number of these studies seriously considered the role of the enhanced density resulting from the compressed phase in the nanofluid, influencing the overall density of the mixture [31,32]. However, these studies were hindered by major shortcomings, and they are discussed as follows:

(a) Measurement uncertainty analyses were either not documented or they were riddled with several errors. For instance, a study incorrectly asserted that the measurement uncertainty for density was between 0.012% and 0.016% [32]. This highlights a misunderstanding on the part of the authors, as they failed to demonstrate experimental repeatability and neglected to derive statistical uncertainty values for the measurements.
(b) Several articles reported a hike in the deviant density component as the mass fraction of the nanoparticles increased. Nevertheless, the theoretical basis for this phenomenon remained uninvestigated or unsubstantiated [27].
(c) With the exception of a single study [29], all research endeavors examined nanoparticles with diameters exceeding 10 nm, commonly falling within the 40–60 nm range. Analytical models in the literature show that the anomalous density component will be undetectable due to the dominance of measurement uncertainty values, especially for nanoparticles with diameters exceeding 12 nm. Solely one study [29] documented density evaluations in an aqueous nanofluid, using alumina nanoparticles with diameters under 10 nm and an atypical density of 6 mg/cc or 0.6%. The apparatus used for these measurements reportedly had a precision of 0.1 mg/cc.
(d) The density of the nanoparticles exceeded 1 g/cc in all these investigations, frequently falling within the range of 2–6 g/cc [27,30]. It will be demonstrated later in the present study that the anticipated anomalous density factor will be notably higher than the measurement uncertainty values (corresponding to a statistical significance of 95%) for nanoparticles possessing densities below 1 g/cc.
(e) Certain studies utilized nanoparticle mass fractions exceeding 5%. However, these results are dubious due to the prevailing influence of agglomeration kinetics, which potentially risks the stability of nanoparticles at higher mass fractions. Therefore, it is often preferable to conduct experiments with nanoparticle mass fractions below 2% (preferably 1% or lower) [27,31].
(f) In one of the studies, the researchers used two sets of instruments for making the same density measurement but happened to report only a single set of density measurements [30]. Hence, the credibility of their findings remains subjective due to potential mismatches between the two sets of measurements (that were never reported).
(g) It was shown by a study that in aqueous nanofluids, the specific heat capacity is lower than that of the solvent because of the deviant density component [30] and this leads to the violation of the simple mixing rule.
(h) There is a void space (having a thickness of approximately 5 Å, comparable to the equilibrium intermolecular spacing values) that separates the surface of the nanoparticle from the solvent molecules in the compressed phase [33,34]. Yet, one of the studies overlooked the extent of the vacant volume between the nanoparticle and the compressed phase [32]. It was wrongly asserted by the authors that void space increases with the size of the nanoparticles and they even suggested it could reach up to 1.3 nm, surpassing the values of equilibrium intermolecular spacing. The correlation established within this research suggests that when particle size increases, the size of the compressed phase also increases. This finding goes against the notion that nanoparticles significantly enhance density to a greater extent than micron-scale particles do. The graphs depicting the comparison of experimental data are unclear, as they fall within the range between predictions generated by the mixing rule and those originating from the flawed model created by the authors.
(i) A study considered the impacts of agglomeration, where secondary nanostructures are anticipated to have a significant influence and would spread throughout the entire volume between nanoparticle clusters [31]. However, the authors overlooked prior findings in existing literature that leveraged electron microscopy images to clearly illustrate the compressed layer that fills the space between clusters of closely-spaced nanoparticles. Even more, they based their hypothesis on the assumption that the presence of the compressed phase was limited only to the periphery of the cluster rather than within it. This could lead to a significant underestimation (of the effects of the closely-spaced cluster of nanoparticles) by several orders of magnitude. In situations where the density values surpassed 1100 kg/m^3, the density values were reported to the fourth decimal place. Such lack of attention to detail renders these reports to be dubious, thus necessitating the need to verify the validity of these results and making the readers desirous of cross-checking these results.

The shortcomings of the simple mixing rule in terms of its ability to precisely estimate nanofluid densities have been frequently discussed in various research articles. Kuchibhotla et al. [4] proposed a novel model for predicting the net density of nanofluids and it incorporated the effect of the interfacial phenomena (at the solid-liquid interface). Their proposed model, which explained the phenomenon of surplus density in pure solvents, holds practical significance for various applications involving nanofluids. These applications include the use of nanofluids as cooling agents and for storing thermal energy (e.g., in the form of sensible heat stored in molten salt nanofluids or in the form of latent heat in phase change materials (PCM)). Additionally, this model is relevant for industries that utilize nanofluids as lubricants due to their unique rheological properties, such as shear-thinning or shear-thickening behavior. Furthermore, it has implications for industrial-grade solvents, space exploration, and nuclear energy. The model can help in the design of systems for transporting densified hydrocarbons, like LNG, e.g., for pipelines and shipping (oil tankers).

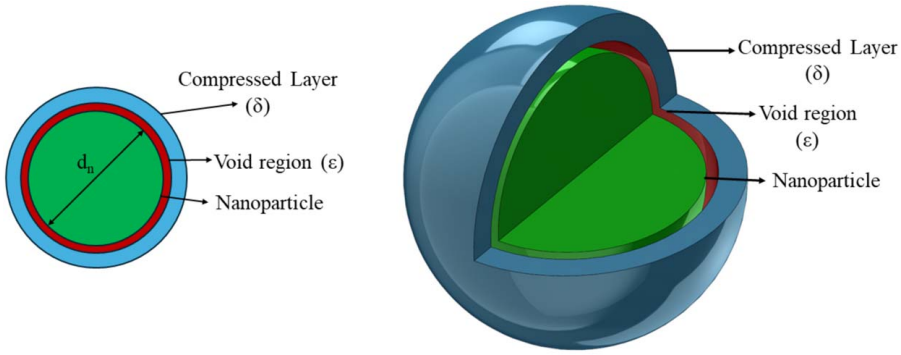

Fig. 1 Schematic of a spherical nanoparticle surrounded by a compressed layer

Importantly, densified fluids can act as radiation shields during space travel (e.g., for astronaut capsules in these space vehicles) and can help mitigate the ill effects of extra-terrestrial radiation for the astronauts. As soon as a space vehicle enters the LEO, it loses the natural protection provided by the Earth's atmosphere against solar and cosmic radiation. Upon entry into deep space, the radiation shielding provided by the Earth's magnetic field is further lost by the spacecraft. The human body is highly vulnerable to serious damage due to the high-energy ionizing radiation in deep space. The radiation can affect the skin, the gastrointestinal tract, the skeletal system, the central nervous system, and the blood-generating organs [35]. Hence, one of the foremost challenges facing the global space community is how to mitigate the ill effects of space radiation on the health of astronauts. Space agencies around the world are investing significant resources to solve the conundrum of space radiation since it is one of the major obstacles preventing mankind from traveling to the farther ends of the solar system. NASA's "Radiation Health Program" aims to improve astronaut conditions to "live and work safely" in space [35].

Hydrogen-rich polyethylene (density varying between 0.93 g/cc and 0.97 g/cc [36]) is used as a shielding material in the International Space Station (ISS) to protect the crew from exposure to space radiation—particularly in frequently occupied zones such as the galley and the sleeping quarters. Narici et al. [37] experimentally investigated the radiation shielding performance of Kevlar, a carbon-rich polymer, onboard the ISS. They found that the performance of Kevlar as a radiation shield is comparable to polyethylene shields—achieving a dose reduction rate of $32 \pm 2\%$ and a dose equivalent rate reduction of $55 \pm 4\%$ (for a shield of 10 g/cm^2). Singleterry conducted a numerical study using the OLTARIS tool to assess the performance of different materials as radiation shields as a function of the optimum period of stay for an astronaut in deep space. Through the study, the author demonstrated that while liquid hydrogen (having a typical density of 0.07 g/cc) itself is not a good shielding material, particularly for space missions exceeding 225 days, densified liquid hydrogen (having a density of 1 g/cc) serves as a better radiation resisting material whose performance is better than liquid water (even though their densities are comparable). Also, hydrogen-stored boron shows good neutron shielding capability [38]. These studies, therefore, indicate that densified hydrocarbons (such as PCM oil-based nanofluids) have strong potential for use as space radiation shielding materials. The phenomenon of density variation in nanofluids, however, has frequently violated the conventional mixing rule.

Despite being the first reported work to investigate the phenomenon of anomalous density variation in oil-based nanofluids—the experimental techniques (such as nanofluid synthesis protocol and the corresponding density measurements) employed by Kuchibhotla et al. [4] to validate the deviant density model for nanofluids had numerous inconsistencies (discussed in the subsequent section) which the current study tries to improve. The standardized nanofluid synthesis protocol and experimental measurement procedures developed in this study that address these deficiencies are discussed next.

2 Methodology

2.1 Analytical Model. Researchers have frequently employed the simple mixing rule, a traditional approach that utilizes the statistical mechanics of ideal gas mixtures, to estimate the net density of nanofluids [39]. This rule relies on the mass concentration of the ingredients and does not take into account the impact of particle size, geometry (morphology and shape), and distribution of particle size and surface phenomenon. As per the principles of classical mixing theory, the effective density (ρ_{T1}) of a mixture, which is composed of both a solvent phase and suspended solid particles, is determined solely by the density of the pure solvent phase (ρ_f), along with the density of the solid phase or nanoparticles (ρ_n), and their respective mass fractions (x), alternatively expressed as the particle volume fraction (φ).

In their study, Kuchibhotla et al. [4] employed a simple mathematical model to explain the interfacial phenomenon occurring at the solid-liquid interface. Their model considers a collection of spherical nanoparticles evenly distributed within a liquid phase (solvent), and it is based on the underlying assumption that each nanoparticle is surrounded by a compressed layer of solvent molecules bearing an approximate thickness (δ). Figure 1 shows the schematic of a nanoparticle enveloped by the compressed phase (descriptive of the model proposed by Kuchibhotla et al. [4]). The authors hypothesized that there exists an intervening "void space" (ε), which is on a similar scale as the equilibrium spacing resulting from intermolecular forces like Van der Waals attractions and ionic repulsions. It was postulated that this void space separates the surface of the spherical nanoparticle from the compressed solvent phase, which presumably encloses each nanoparticle within an envelope. As a result, the primary factor influencing the effective density of the nanofluids is thought to be a compressed layer of solvent molecules (with a nominal thickness of 1–2 nm). This layer is accompanied by a void region (ε) having an approximate thickness of 0.5 nm, and it is assumed to be present between the compressed region and the surface of the nanoparticle.

As per the analytical model (alternatively labeled as the compressed phase model), the effective nanofluid density (ρ_{T2}) is considered to be influenced by a combination of individual density components—namely, the increased density of the compressed phase (ρ_c), the density of the bulk phase of the base solvent (ρ_f), and the density of the nanoparticle (ρ_n). The corresponding mass concentrations of these individual constituents (nanoparticle, bulk solvent phase, and compressed phase) also affect the density of the mixture (ρ_{T2}). Parametric variation is performed for the mass fraction and particle size of the compressed phase, as determined by data extracted from experimental measurements documented in the literature [40] regarding compressed phase thickness, along with numerical forecasts from the literature [6,7] regarding compressed phase density (which was estimated through molecular dynamics simulations). Using the analytical model, the net density (or corresponding specific volume) of the nanofluid can be calculated as

$$\frac{1}{\rho_{T2}} = \frac{x}{\rho_n} + \frac{y}{\rho_c} + \frac{(1-x-y)}{\rho_f}; \qquad v_{T2} = xv_n + yv_c + (1-x-y)v_f \tag{1}$$

where ρ_{T2} represents the effective density of the nanofluid (involving compressed phase), x and y are mass fractions of nanoparticles and compressed phase respectively, ρ_c is the compressed phase density, ρ_n refers to the density of the nanoparticles, and ρ_f refers to the density of the bulk phase of the base solvent, v_{T2} represents the effective specific volume of the nanofluid (including the compressed phase). Also, v_C, v_n, and v_f refer to the specific volumes of the compressed phase, the nanoparticle, and the bulk phase of the base solvent, respectively.

On the other hand, the estimate for the effective nanofluid density, ρ_{T1},(or specific volume, v_{T1}) can be obtained using the traditional simple mixing rule, as shown follows:

$$\frac{1}{\rho_{T1}} = \frac{x}{\rho_n} + \frac{(1-x)}{\rho_f}; \quad v_{T1} = xv_n + (1-x)v_f \tag{2}$$

Kuchibhotla et al. [4] presented a detailed derivation of the deviation density formulation. Effectively, the excess contribution to the values of density, or specific volume, which surpasses the anticipated values estimated using the simple mixing rule is given as

$$\rho_{T21} = \rho_{T2} - \rho_{T1}; \quad v_{T21} = v_{T2} - v_{T1} \tag{3}$$

The excess contribution to the specific volume with respect to the anticipated value yielded by the conventional simple mixing rule can be expressed in terms of the relative deviation as

$$\Delta_{V21} = \frac{v_{T2} - v_{T1}}{v_{T1}} \tag{4}$$

The expression above can also be used to estimate the deviant density of the nanofluid sample. Following the numerical derivation presented by Kuchibhotla et al., Eq. (4) can be alternatively expressed in the following manner:

$$\Delta_{V21} = -\frac{x\left(\frac{\rho_c}{\rho_n}\right)\left[1-\left(\frac{\rho_f}{\rho_c}\right)\right]\left(\frac{V_c}{V_n}\right)}{1-x\left[1-\left(\frac{\rho_f}{\rho_n}\right)\right]}; \qquad \frac{\Delta_{V21}}{x} = -\frac{\left(\frac{\rho_c}{\rho_n}\right)\left[1-\left(\frac{\rho_f}{\rho_c}\right)\right]\left(\frac{V_c}{V_n}\right)}{1-x\left[1-\left(\frac{\rho_f}{\rho_n}\right)\right]} \tag{5}$$

where V_n refers to the volume of a nanoparticle and V_c represents the net volume of the compressed phase.

It is clear from Eq. (5) that the magnitude of Δ_{V21} reaches its maximum value (as in, the surplus or deviant density term is amplified) on either maximizing the numerator or minimizing the denominator. Therefore, the magnitude of Δ_{V21} can be maximized under the following conditions:

(1) The magnitude of ρ_n needs to be minimized. In simple terms, the specific gravity of the nanoparticles should be very low, desirably smaller than 1.
(2) The magnitude of ρ_c is required to be very high. Desirably, the specific gravity of the compressed phase formed by the solvent molecules should be greater than 1. Consequently, the use of aqueous nanofluids is not considered viable since the anticipated characteristics of the compressed phase formed by water molecules on the nanoparticle surface resemble the properties of ice, which generally has a specific gravity below 1.
(3) The magnitude of ρ_f is required to be very low. In effect, the liquid phase density of the base solvent should desirably be smaller than 1.
(4) The term $\left(\frac{\rho_f}{\rho_c}\right)$ should have a value less than 1. In other words, the liquid phase density of the base solvent should be less than the solid phase density. Consequently, the use of aqueous nanofluids is not considered viable since the anticipated characteristics of the compressed phase created by water molecules on the nanoparticle surface resemble the properties of ice, which generally exhibits a specific gravity below 1.
(5) The compressed phase volume is required to be maximized. In other words, it is desirable that the volume of the compressed phase should be maximized.
(6) The size of the nanoparticle (and consequently its volume) is required to be very small.

The above discussion on surplus density emphasizes the necessity for meticulous design of experiments for effectively identifying and measuring the deviant component of the density enhancement that is expected to arise from the formation of the compressed phase within the solvent (and on the surface of the nanoparticle). At the same time, attention should be directed toward minimizing measurement uncertainty to conclusively estimate the contribution of the deviant density component to the overall enhancement in the measured values of the density of the nanofluids. Hence, this has a profound effect on the selection of the solvent materials, which is discussed next.

2.2 Selection of Solvent Candidates. The findings of the MD simulations [7] indicate that the density of the compressed phase is generally 25–100% greater (almost twice as much) compared to the density of the base solvent. This difference is particularly pronounced in non-aqueous solvents, such as organic solvents, and is especially significant for oil-based solvents and molten salt eutectics. Hence, taking cue from these behavioral trends as documented in the literature involving MD simulations, Kuchibhotla et al. selected oil-based solvent candidates in their nanofluid synthesis protocol. They chose a paraffin-based oil (typically used as a PCM), available commercially as PureTemp-15X (procured from PureTemp), that was used for their study. Under the assumption that the ratio of the densities of the compressed phase and the liquid phase of the base solvent, $\left(\frac{\rho_c}{\rho_f}\right)$, approximately equals two, the relative deviation in the specific volume of the nanofluid can be expressed as

$$\Delta_{V21} = -\frac{x\left(\frac{\rho_c}{\rho_n}\right)\left(\frac{V_c}{V_n}\right)A}{1-x\left[1-\left(\frac{\rho_f}{\rho_n}\right)\right]} \tag{6}$$

where A is the correction factor whose approximate value for oils is 0.5. On the other hand, the density ratio between the compressed phase and the liquid phase, $\left(\frac{\rho_c}{\rho_f}\right)$, approximately equals 0.9 for water [9], because the specific gravity of ice is 0.9. Consequently, when water is used as the base fluid, a positive value is obtained from the relative surplus specific volume term (thus, leading to a marginal decrease in the density of aqueous nanofluids, instead of the enhancements that are observed for non-aqueous nanofluids). The relative deviation in the specific volume of aqueous nanofluids can be expressed as

$$\Delta_{V21} = -\frac{x\left(\frac{\rho_c}{\rho_n}\right)\left(\frac{V_c}{V_n}\right)B}{1-x\left[1-\left(\frac{\rho_f}{\rho_n}\right)\right]} \tag{7}$$

where B represents the corresponding correction factor, and it approximates a value of −0.1.

Therefore, the phenomenon of anomalous density (or surplus density) resulting from the formation of the compressed layer is less likely to be acutely observable in nanofluids synthesized using water as the base fluid. Moreover, the density of water-based nanofluids is more inclined to adhere to the simple mixing rule, even when dealing with nanoparticles with diameters less than 6 nm. Consequently, water-based nanofluids are likely to have a tiny decrease in density with respect to the estimates obtained from the simple mixing rule. Moreover, the reduction in the deviant density is so small for aqueous nanofluids (approximated to be less than 0.5%), that the change cannot be practically perceived by conventional density measurement apparatus or even by commercial instruments designed for the same purpose (such as densitometers). Nevertheless, important inferences can be drawn for the specific heat capacity of aqueous nanofluids from these analyses. This also suggests that identifying the anomalous values of specific heat capacity (or excessive values of specific heat capacity) resulting from the compressed layer is nearly impossible in experiments involving aqueous nanofluids. The specific heat capacity of these nanofluids is more likely to follow the conventional simple mixing rule. Consequently, there might be a slight decrease (below 2%) in the specific heat capacity values of aqueous nanofluids, even for nanoparticles with diameters less than 6 nm. However, detecting such a small depreciation is challenging, given that the standard measurement uncertainty associated with specific heat capacity measurements (such as by employing techniques like differential scanning calorimetry) is roughly 5% or more. Interestingly, several research articles (such as Ref. [30]) revealed a decline in the specific heat capacity of nanofluid samples based in water. These values were consistently lower than the estimates predicted by the simple mixing rule.

2.3 Selection of Nanoparticle Candidates. Prior to performing the experimental measurements, the density or thickness of the compressed phase is unknown (molecular dynamic simulations could only provide approximate predictions). Besides, these thermophysical property values are highly sensitive to even small changes in the synthesis conditions (such as pH of the medium, concentration of surfactants, temperature at which synthesis is performed, etc.). Under such circumstances, the density of the nanoparticles serves as the most important control variable in the synthesis protocol. Hence, the nanoparticle density should be minimized in the design of experiments and the choice of the synthesis protocol.

A dilemma arises from this situation, as the traditional nanoparticles typically employed in the nanofluid literature (like metallic, ceramic, or carbon-based nanoparticles) usually possess specific gravity values exceeding two [41]. Generally, ceramic nanoparticles, like silica and alumina, typically exhibit a specific gravity of around two. On the other hand, metallic nanoparticles such as tungsten, gold, and silver, tend to have even higher specific gravity values, frequently surpassing two. Carbon nanoparticles exhibit a specific gravity that usually surpasses two (for instance, 2.2 for graphene, 3.5 for exfoliated graphite, 1.4 for carbon nanotubes, and 3.4 for diamond nanoparticles). Among these, carbon nanotubes have the lowest specific gravity; however, they pose a significant challenge for synthesizing stable dispersions in conventional solvents. Hence, obtaining stable colloidal dispersions from these conventional nanoparticle candidates remains quite challenging, whether they are aqueous nanofluids or oil-based nanofluids (oleo-nanofluids).

A quick literature study shows that complex organic nanoparticles, including proteins, lipids/vesicles, etc., exhibit a specific gravity below one. Generally, these values fall within the range of 0.4–0.9 [42]. However, these nanoparticles are very expensive. Also, chemical or material stability is often challenging for proteins (and likewise, for lipids/vesicles) as they have the innate tendency to spontaneously denature when subjected to thermal shocks or mechanical stresses, or when exposed to shear forces or chemical gradients.

In contrast, the proteins derived from dehydrated skim milk are mainly comprised of the protein called "casein." Casein shows remarkable thermal stability (and therefore is often used as an additive in food processing applications). Furthermore, casein can readily dissolve in either water or oil. The anticipated Stokes diameter of casein, similar to other proteins and peptides, is projected to range from 2 nm to 6 nm (which is ideal for the chosen design of experiments in this study). The specific gravity of Casein spans from 0.45 to 0.5 (depending on the size of the protein) [42]. This variation is dependent on the sizes of the complexes created between surfactants and proteins, as well as the varying degrees of hydration for the protein molecules in a hydrated state. Therefore, Kuchibhotla et al. [4] selected casein [43,44], as the nanoparticle candidate in their investigation (which was easily available in the form of dehydrated non-fat skimmed milk). In their experimental study, they used paraffin-based oil (PureTemp-15X) as the base solvent and selected casein as the low-density nanoparticle candidate (because the specific gravity of this class of proteins is less than 1). However, despite the attention to detail, their study lacked proper design of experiments. The fluid that was synthesized using their proposed procedure and thereafter tested for density measurement is expected to be mixed with both water and oil present in the samples, which violated the fundamental need that the test fluid samples must be non-aqueous in nature. The same anomaly trickled down to their simple mixing rule estimation of nanofluid density, where the effect of water as a constituent was considered. The authors claimed that casein nanoparticles were present in the fluid medium, but they failed to provide any substantial evidence (such as microscopy images) to physically validate their claim. Furthermore, though they demonstrated the presence of a "surplus" density component in oleo-nanofluids and attributed this anomaly to the presence of a compressed phase engulfing the nanoparticles, they failed to physically characterize the extent of the compressed layers in the synthesized oleo-nanofluid samples. Their published work demonstrated numerous discrepancies in the nanofluid synthesis protocol, indicating a lack of precision in controlling the input conditions.

The existing synthesis protocol for oil-based nanofluids was standardized in this study. Transmission electronic microscopy (TEM) of the test fluid samples is thereafter performed in this study to visualize the size of the nanoparticles (and estimate the contribution of the associated secondary nanostructures such as the compressed phase) and also to determine the particle size distribution of the nanostructures in the oleo-nanofluid samples.

3 Experimental Apparatus and Procedure

3.1 Synthesis Protocol. The protocol established by Kuchibhotla et al. [4] for synthesizing casein-protein doped oleo-nanofluids is implemented in this study as well. Several standardization measures were incorporated into this previously existing protocol in order to exercise additional control over the synthesis process. Figure 2 illustrates the synthesis protocol for oleo-nanofluids and this is described next:

(i) Preparation of aqueous solution: sodium dodecyl sulfate (SDS) is added to a beaker containing de-ionized water and stirred manually. When SDS is completely dissolved in water, the beaker is kept in a larger pot and ice cubes are introduced around the beaker. Thereafter, sodium hydroxide (NaOH) and milk powder are respectively introduced into the aqueous solution in small batches while manually stirring the beaker at a gentle pace. Stirring is continued till the added ingredients are dissolved completely in the aqueous solution—each time after dispensing them into the beaker.
(ii) Preparation of oil solution: SDS is added to oil (neat solvent) and stirred gently.

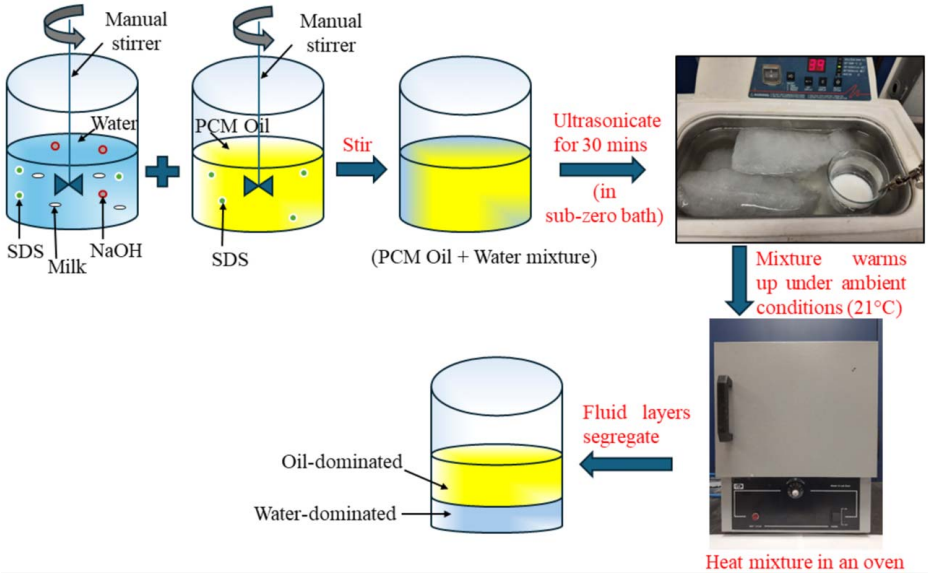

Fig. 2 Schematic diagram of the synthesis process of oleo-nanofluids: casein nanoparticles in the PCM oil

(iii) The oil and aqueous solutions are mixed until a reasonably consistent white mixture is achieved. The beaker is stirred well to ensure that no oil is visible on top of the beaker.

(iv) 500 g common salt is added in 5000 ml water to get a freezing point depression of 6.4 °C. A substantial amount of this solution is frozen for preparing the subzero ice bath, while the remaining is used to fill up the ultrasonicator. A Branson 3510MT ultrasonicc, which has a capacity of 1.5 gallons and an operating frequency of 40 Hz is used for ultrasonicating the mixture.

(v) Ultrasonication: The salted ice cubes are dispensed into the water bath of the ultrasonicator. The beaker containing the sample is then immersed into the frozen ice cubes and the contents within the beaker are ultra-sonicated in this subzero ice bath for 30 min to enable finer mixing of the ingredients. Ultrasonication is activated (and likewise, deactivated) by pressing the ON/OFF switch.

(vi) On completing ultrasonication, a substantial time (18–20 h) is allowed for the nanofluid sample (that was exposed to subzero conditions in the ultrasonicator) to warm up to the ambient conditions.

(vii) Oven heating: The oven is preheated for 2 h, such that a steady-state temperature regime at 55 ± 2 °C is established within the control volume of the oven. Thereafter, the fluid sample is placed inside the oven under heating mode. After an hour, the temperature of the oven is lowered to attain a new steady-state temperature of 41 ± 2 °C. In this temperature regime, the beaker is kept inside the oven for another 90 min. Oven heating enables the homogeneous fluid mixture in the beaker to segregate into two distinct layers —the top portion is oil-dominated (oil solution, i.e., PCM layer) and the bottom portion is dominated by aqueous solution.

(viii) After completion of the heating cycle in the oven, the beaker is taken out of the oven and allowed to cool under ambient conditions (at room temperature) for 90 min and thereafter the fluid densities are measured at room temperature. Hence, sufficient time is allowed for the fluid to cool down from 40 °C to room temperature conditions (i.e., 21 °C). Figure 3(*a*) shows the image of the beaker containing the test fluid prior to subjecting the beaker to oven heating. In this stage of synthesis, the test fluid is visually apparent to be homogenous. Figure 3(*b*) shows a clear separation of the oil solution and aqueous solutions in the beaker after the sample is taken out of the oven at the end of the heating period.

The oil-dominated oleo-nanofluid layer at the top of the beaker is the region of interest as we are seeking to investigate the density

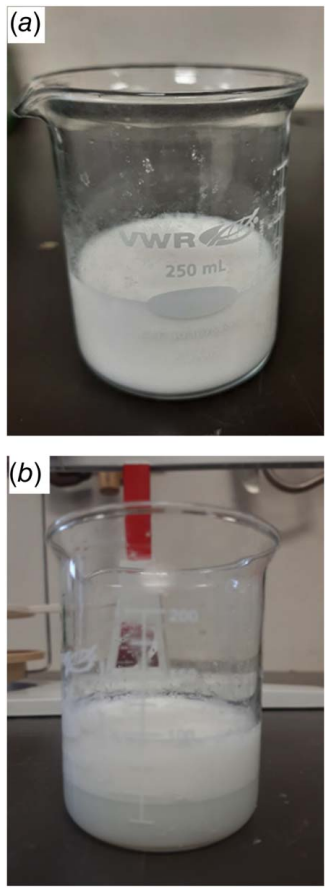

Fig. 3 (*a*) Test fluid sample prior to oven heating and (*b*) test fluid sample after oven heating showing segregated two distinct layers (oleo-nanofluid and aqueous nanofluid)

variations in non-aqueous nanofluids. Fluid samples are extracted from both the oil-dominated top layer (oleo-nanofluid sample) and the aqueous solution in the bottom of the beaker (using pipettes) and their corresponding densities are measured. Table 1 lists the masses of the ingredients used in the synthesis protocol. It may be noted that the density of SDS is 1.01 g/cc [4] and the density of NaOH is 2.13 g/cc [45].

3.2 Experimental Apparatus. Figure 4 shows the Ohaus 310-00 Dial-o-gram mechanical balance which has been used in this study for measuring the densities of the test fluids (based on the Archimedean principle of buoyancy of immersed bodies). The device has a least count of 0.01 g. A "sinker" is suspended from the free end of the balance arm with the help of a wire.

The buoyancy force experienced by the sinker when suspended in a certain fluid can be quantified by measuring the difference in weights for the sinker suspended in the fluid compared to its weight in the air.

When the sinker is submerged in water at room temperature (21 °C), the density of water, ρ_w, would be

$$\rho_w = \frac{\rho_s \times (m_a - m_w)}{m_a} \tag{8}$$

where ρ_s is the density of the sinker, m_a is the mass of the sinker when suspended in air, and m_w is the mass of the sinker in water.

Similarly, the density of a test fluid *tf* (i.e., the fluid whose density is required to be determined) can be obtained in the following way:

$$\rho_{tf} = \frac{\rho_s \times (m_a - m_{tf})}{m_a} \tag{9}$$

where ρ_{tf} is the density of the test fluid, and m_{tf} is the mass of the sinker when suspended in the test fluid.

Dividing Eq. (9) by Eq. (8) would yield the mode; for estimating the density of the test fluid as a function of the density of water (i.e., the values of specific gravity of the test fluid).

$$\frac{\rho_{tf}}{\rho_w} = \frac{(m_a - m_{tf})}{(m_a - m_w)} \tag{10}$$

In the present study, all the measurements were performed under ambient conditions (at a room temperature of 21 °C). The density of water at this temperature is 0.998 g/cc [46].

3.3 Uncertainty Analysis. The Kline–McClintock method [8] is used to quantify the uncertainty values of the experimental measurements. The bias uncertainty in measurement, or the bias error (instrument error) is 50% of the least count of the mass measuring device. Three repeat tests are performed. The sinker's weight is measured six times while it is suspended in air, water, or a fluid sample, and the statistical uncertainty reported corresponds to a 95% confidence interval.

The uncertainty in the mass of the sinker when suspended in a given fluid medium *i* (i.e., u_{m_i}) is given as follows:

$$u_{m_i} = [(u_{m_i})^2_{bias} + (u_{m_i})^2_{stat}]^{1/2} \tag{11}$$

Table 1 Mass of ingredients used for the synthesis of oleo-nanofluid samples

Solutions	Component	Mass (g)
Water solution	Water	40
	SDS	0.2
	NaOH	0.4
	Milk powder	0.4
Oil solution	Oil (PCM)	40
	SDS	0.2

where $(u_{m_i})_{\text{bias}}$ and $(u_{m_i})_{\text{stat}}$ are the bias and statistical errors respectively in the mass measurement.

The error in the difference between two measured masses m_i and m_j is given by

$$u_{\Delta m_{i-j}} = u_{m_i} + u_{m_j} \tag{12}$$

where Δm_{i-j} is the difference in the mass of the sinker when suspended in mediums *i* and *j* respectively.

Following Eq. (10), the overall relative error in the density of the test fluid can be determined by computing the square root of the sum of squares of the relative errors in the mass defects of the sinker in water $(m_a - m_w)$ and the test fluid $(m_a - m_{tf})$ versus its mass in air.

$$\frac{u_{\rho_{tf}}}{\rho_{tf}} = \left[\left(\frac{u_{\Delta m_{a-w}}}{\Delta m_{a-w}}\right)^2 + \left(\frac{u_{\Delta m_{a-tf}}}{\Delta m_{a-tf}}\right)^2\right]^{1/2} \tag{13}$$

Hence, these equations can be used to estimate the measurement uncertainty for the values of density. The validity of these models is supplemented by TEM images, which is described next.

3.4 Transmission Electron Microscopy Imaging of Oleo-Nanofluid Samples. TEM (at room temperature) is used to assess the appearance and dimensions of the nanostructures present in the oil-dominated test fluid. Serially diluted samples of the test fluid are prepared in dilution ratios (by volume) of 1:1, 1:2, and 1:100. De-ionized water is used as the dilution agent. Each fluid sample is mounted on a support film of Formvar-coated carbon on 400 copper mesh grids, procured from electron microscopy sciences. Prior to mounting the fluid samples, the grids are subjected to glow discharging with the help of PELCO easiGlow

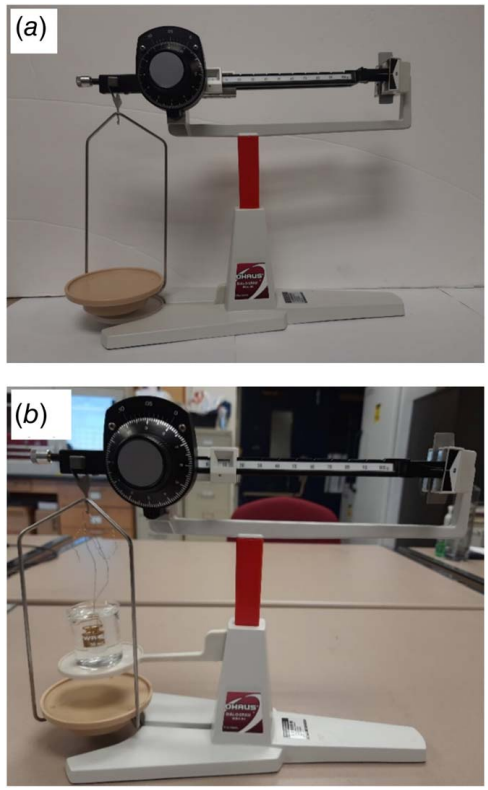

Fig. 4 (*a*) Image of the mass balance used for measuring fluid densities using the principle of buoyancy, (*b*) the mass balance is used to measure the mass of the sinker when suspended in air, water, and the test fluid (as shown in the figure) and the Archimedean principle of buoyancy is thereafter applied to obtain the fluid densities.

Table 2 Simple mixing rule prediction (considering contributions from milk protein and PCM oil)

Ingredient	Mass (g)	Mass fraction, x_i	Density ρ_i (g/cc)	$\frac{x_i}{\rho_i}$	$\sum \frac{x_i}{\rho_i}$	ρ_{T1} (g/cc)
PCM oil	40	0.99	0.86	1.151	1.171	0.85
Milk powder	0.4	0.01	0.5	0.02		

Table 3 Uncertainty in the measured mass of the sinker in air

Mass of the sinker in air (g)	Measurement uncertainty (g)	Statistical uncertainty (g)	Overall uncertainty, u_{m_a} (g)
20.36	0.005	0.008	0.009

Table 4 Uncertainty in the measured mass of the sinker in water

Mass of the sinker in water (g)	Measurement uncertainty (g)	Statistical uncertainty (g)	Overall uncertainty, u_{m_w} (g)
18.01	0.005	0.01	0.011

Table 5 Benchmark results using mineral oil

Mass in air (g)	Mass in water (g)	Mass in oil (g)	Measured density of mineral oil (g/cc)	Standard density value (g/cc)	Deviation (%)
20.36	18.01	18.33	0.86	0.85	1.18

glow discharge cleaning system. This helps in removing atmospheric contaminants and making the grids hydrophilic. TEM grids are prepared for a given dilution factor—one set is stained with a 2% uranyl acetate solution (pH undetermined) while the other set of grids is unstained. The grids are imaged with a FEI TECNAI G2 F20 FE-TEM at an accelerating voltage of 200 kV.

3.5 Computational Analysis of Transmission Electron Microscopy Images. The image processing software BSOFT [47] and IMAGEJ [48] are employed for processing the TEM images and characterizing the variation of gray-value intensity in the imaged nanofluids. The particle size distribution in the nanostructures is determined using two different approaches—namely, by performing a fast Fourier transform analysis (FFT) of the region of interest with the help of the image processing software BSOFT and by measuring the mean pixel size of the nanoparticles using IMAGEJ.

The TEM image of the nanofluid sample is computationally boxed out (with box size 256×256 pixels, where 1 pixel = 2.56 Å). FFT of all the boxes are generated using the program bfft of the software package BSOFT. An averaged FFT image is generated by adding the individual FFT images using the program bop of the BSOFT package. The repeatability of the nanostructures can be obtained from the average FFT image of the nanofluid sample.

A secondary approach for particle size measurement is also implemented using IMAGEJ. It typically involves employing a line to traverse along the particle's surface, yielding linear measurements for each particle. Moreover, a distribution of the particle sizes for 100 measured lengths is plotted in a histogram and thereafter, a Gaussian curve is fitted to the graph using the software ORIGINPRO. The fit is obtained by allowing the software to iterate till convergence. In the present study, 12 iterations are taken by the software to converge to a steady solution and a best fit is obtained.

A gray-value profiling of the TEM images is performed in IMAGEJ to characterize the density variation in the imaged oleo-nanofluid sample.

4 Results and Discussion

Density prediction as per simple mixing rule

Table 2 shows the density (ρ_{T1}) of the nanofluid obtained following the simple mixing rule with the fluid medium containing casein nanoparticles and PCM. This estimated density value (ρ_{T1}) of 0.85 g/cc is considered as the baseline prediction in all the subsequent calculations hereafter.

4.1 Uncertainties in the Mass of the Sinker in Air and Water. Tables 3 and 4 list the uncertainties in the mass of the sinker when suspended in air and water respectively. The measured mass reported in each case is an average of six mass readings. These results are required for quantifying the uncertainties in the measured nanofluid densities, using Eqs. (11)–(13).

4.2 Calibration of the Mass Balance Apparatus. Prior to measuring the densities of the oleo-nanofluid samples, the experimental apparatus is calibrated by measuring the density of mineral oil, which has a known value of density under ambient conditions (i.e., at 21 °C).

Table 5 summarizes the results obtained from the benchmark test that is conducted using mineral oil-based upon six readings of the mass of the sinker in the oil. The result indicates that the measured value deviated from the value listed in the ASTM standard database by 1.18%. Hence, for measurements involving oil samples, the deviation in the measured value from the true value is expected to be less than 1.2%. The densities of the samples of oleo-nanofluids are measured following the benchmark test.

4.3 Density Measurement Results. Table 6 shows the measured density of the oleo-nanofluid samples extracted from the top layer in the beaker. Density measurements were performed for three repeat samples that were each synthesized following the same procedure. As indicated by the results, the experimental measurements are repeatable within agreeable thresholds of

Table 6 Measured density of the oleo-nanofluid samples extracted from the top layer of the beaker

Sample	Mass of sinker in the nanofluid sample (g)	Measured density of the nanofluid sample (g/cc)	Uncertainty in the mass of the sinker in the nanofluid, $u_{m_{nf}}$ (g)	Uncertainty in the measured density (%)
1	18.23	0.90	0.017	1.49
2	18.22	0.91	0.016	1.45
3	18.22	0.91	0.016	1.45

Table 7 Deviation in oleo-nanofluid density compared to that of the neat solvent (PCM)

Sample	Density of nanofluid sample (g/cc)	Percentage enhancement from PCM density (%)
1	0.90	4.65 ± 1.51
2	0.91	5.81 ± 1.51
3	0.91	5.81 ± 1.51

Table 8 Deviation from simple mixing rule prediction

Sample	Density of nanofluid sample (g/cc)	Percentage deviation from simple mixing rule (%)
1	0.90	5.88 ± 1.54
2	0.91	7.06 ± 1.53
3	0.91	7.06 ± 1.54

measurement uncertainty values. The results for variations in the densities of the nanofluid samples from that of the neat solvent are listed in Table 7. Clearly, the oleo-nanofluid samples reflect a positive enhancement in density with respect to the neat solvent.

Table 8 presents the disparity between the measured nanofluid density and the forecasted value (ρ_{T1}) derived from the simple mixing rule. As listed in Table 2, the simple mixing rule predicts that the density of the oleo-nanofluid is 0.85 g/cc. A significant difference is present between the measured values of nanofluid density and the values predicted by the simple mixing rule, indicating the presence of an additional phase in the fluid domain (i.e., the compressed phase) which contributes to this unusual increase in the nanofluid density. Table 9 lists the measured density of the fluid samples extracted from the bottom layer of the beaker. The results recorded in all three repeat samples indicate that the fluid contained in the bottom layer of the beaker had a density value very close to the density of water (which has a standard density value of 0.998 g/cc at 21 °C), indicative of the fact that this layer is primarily constituted of composition similar to that of pure water.

4.4 Surplus Density Calculation From the Analytical Model. To determine the contribution of the compressed phase to the overall density of the nanofluid samples in these findings, the predictions from the analytical model were derived by parametrically altering both the size of the nanoparticles and the thickness of the compressed phase. Figure 5 depicts the surplus density predictions from the analytical model. It was assumed that the compressed phase would have an identical specific gravity to the solid phase of the solvent ($\rho_c = 0.95$ g/cc). Similarly, the specific gravity of the liquid phase of the solvent was assumed to match that of the pure solvent at 24 °C ($\rho_f = 0.86$ g/cc) [49]. The graphs were plotted based on the assumption that the thickness of the void space, $\varepsilon = 5$ Å (or 0.5 nm). Two different magnitudes of the compressed layer thickness (δ), i.e., $\delta = 1$ nm and $\delta = 2$ nm were considered. The graphs indicate that with a nanoparticle radius of 1 nm, the surplus density is 2.2% (when $\delta = 1$ nm and $x = 1\%$), whereas the surplus density value is 7.6% (when $\delta = 2$ nm and $x = 1\%$).

Therefore, when comparing the experimental measurements with the numerical predictions, it is anticipated that the thickness of the compressed phase surrounding the protein nanoparticles (casein) falls within the range of 1–2 nm. Moreover, Eq. (5) predicts a more specific value of the compressed layer thickness and is estimated to be 1.9 nm. Hence, the deviant density model predicts that the overall size of the nanoparticle (incorporating the presence of a compressed layer) to be approximately 6.8 nm. Now that the effective nanoparticle size (inclusive of the compressed layer thickness) has been predicted with the help of the deviant density model, it would be interesting to see how the nanoparticle size distribution obtained by analyzing the TEM images of the oleo-nanofluids compared with the dimension estimates suggested by the analytical model. This is described next.

4.5 Transmission Electron Microscopy Imaging of Nanofluid Samples and Analysis. Figures 6(*a*) and 6(*b*) show the TEM images of the PCM oil samples. The image shows dark patches of oil on the face of a lighter grid. In contrast, Fig. 6(*c*) shows the TEM image of oleo-nanofluid sample containing milk proteins (casein) along with the averaged FFT of the different sections of the imaged oleo-nanofluid sample. Prominent nanocrystalline striations are visible on the face of the solvent (PCM oil), markedly reaffirming our hypothesis that the nanoparticles are surrounded by secondary structures that are induced from the surface adsorption of the solvent molecules. These unique features are absent in the images of the control samples in Fig. 6(*a*) and 6(*b*).

Since the nanocrystalline structures are characterized by periodic peaks and troughs having wave-like features, a Fourier transform analysis provides a better estimation of the dimension of these features. The images suggest that the crystalline structures are uniformly distributed throughout the sample and are repeatable, having a size of 5.9 nm (i.e., ~6 nm). Disturbances are seen in a few spots of the image, which could arise possibly from uncertainties introduced during the sample preparation process or because of external forces acting on the sample that damaged the periodicity. The particle size is also determined using IMAGEJ by measuring the distance between two consecutive peaks or troughs within the striations. One hundred particle length measurements have been conducted for determining the particle sizes. The typical dimension of a

Table 9 Measured density of the fluid sample extracted from the bottom half of the beaker

Sample	Mass of sinker in test sample (g)	Measured density of test sample (g/cc)	Uncertainty in the mass of the sinker in test fluid, u_{m_f} (g)	Uncertainty in the measured density (%)
1	18.02	0.99	0.009	1.15
2	18.04	0.99	0.011	1.21
3	18.03	0.99	0.009	1.15

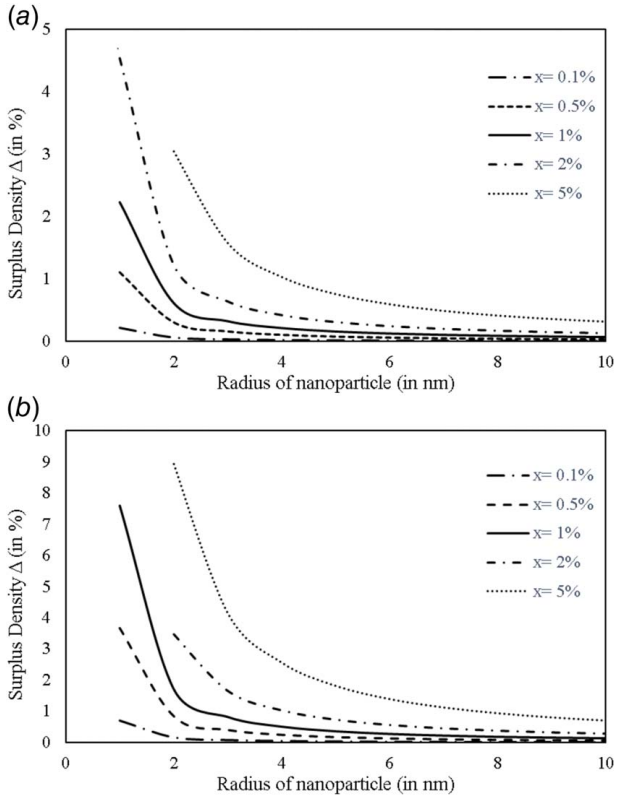

Fig. 5 Graphs illustrating analytical predictions for calculating the effect of "deviant" density (Δ) in an oleo-nanofluid mixture, as a function of the Stokes radius of a nanoparticle (for instance, casein/milk proteins distributed in PCM) for assumed compressed layer thicknesses of (*a*) $\delta = 1$ nm and (*b*) $\delta = 2$ nm. The phenomenon of surplus density (deviant density) is believed to emerge from the existence of a compressed phase that forms on the surface of the nanoparticle due to surface adsorption of the solvent molecules. This phase then surrounds every casein nanoparticle within the overall bulk phase of the solvent (PCM or oil).

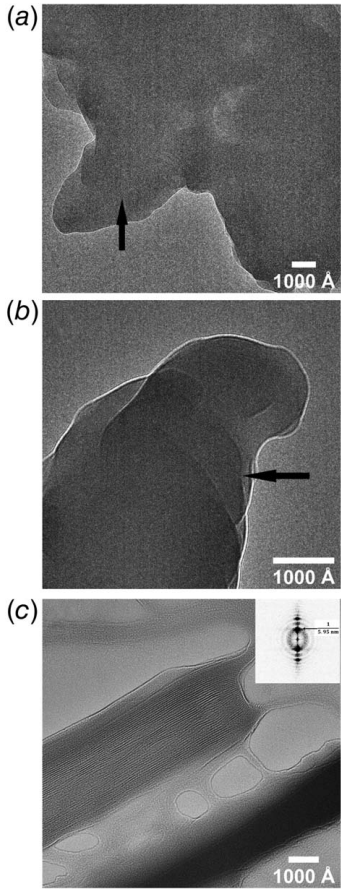

Fig. 6 (*a*), (*b*) TEM images of PCM oil control sample—the dark patches in the images indicated by the arrowheads are essentially paraffin oil samples (void of any added constituent), and (*c*) TEM image of oleo-nanofluid sample along with the averaged FFT of the different sections of the imaged oleo-nanofluid sample

nanocrystal is found to be 6.2 ± 0.6 nm. Figure 7 shows the frequency of nanoparticles falling within various dimension bins, along with the Gaussian curve that is fitted with the help of the software ORIGINPRO. The results from the particle size distribution studies obtained using two different approaches are therefore mutually consistent. Figure 8 depicts the variation in the gray-scale intensity in the images. The presence of periodic density gradients is clearly indicated within the investigated medium, suggesting the presence of nanoparticles whose densities differ from that of the surrounding solvent. The grayscale intensity varies between 25 and 40 within the nanoparticulate agglomerations, with the crests and troughs representing the periodicity in the nanocrystalline structures.

Interestingly, Shin and Banerjee [9] investigated the thermophysical behavior of a eutectic of lithium carbonate and potassium carbonate doped with silica nanoparticles and observed a similar percolation network of high-density eutectic material enveloping the silica nanoparticles in the microscopy images. The density variations in the TEM images in the current study agree well with their findings.

According to the results obtained from the numerical model, a casein nanoparticle in the test fluid domain is supposed to have a Stokes diameter of 2 nm, surrounded by a compressed layer having a thickness of 1.9 nm and an intervening void space of 0.5 nm. To put it simply, the overall dimension of a nanoparticle is predicted to vary between 5 nm and 7 nm (the surplus density formulation given by Eq. (5) suggests that the effective dimension should be 6.8 nm). The particle size distribution data obtained by analyzing the TEM images also seem to conclude that the size of a nanoparticle is 6.2 ± 0.6 nm. In other words, the data from the particle size study agree with the size predictions obtained from the deviant density numerical model. Thus, the particle size distribution study further validates the consistency of the numerical model and confirms the existence of a semi-crystalline compressed layer encompassing the nanoparticles within the oleo-nanofluid domain.

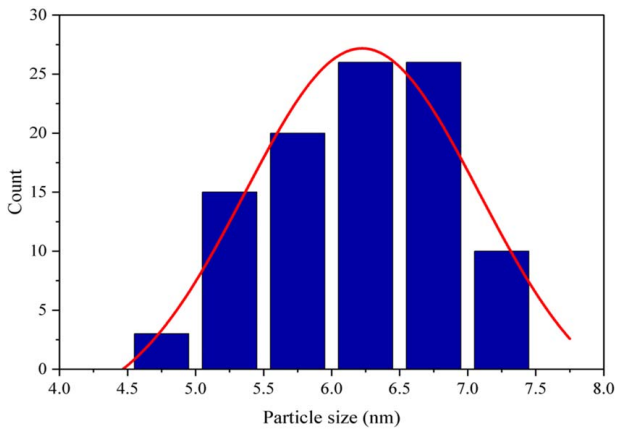

Fig. 7 Particle size distribution of nanocrystalline structures along with the Gaussian fit. The data are based on the image analysis of 100 distinct nanocrystalline striations.

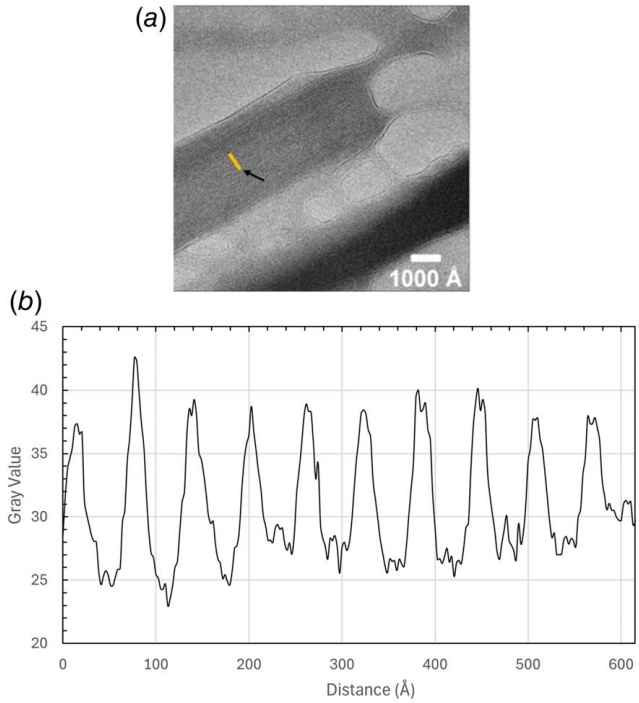

Fig. 8 (*a*) Image of nanofluid analyzed for studying density variation along with (*b*) the corresponding gray-value intensity variation within the imaged nanocrystalline structures across the straight marker (indicated by the arrow)

5 Conclusion

Experimental validation of numerical predictions for the values of surplus density (deviant density) of oleo-nanofluid samples containing casein nanoparticles was carried out. The experimental results and TEM images of nanofluids were leveraged to validate the numerical values predicted by the analytical model for the deviant density, which is consistent with the model proposed by Kuchibhotla et al. [4]. The experimental density measurements indicate that the density of the nanofluid samples differs from the simple mixing rule prediction by 7%. Furthermore, TEM imaging of the nanofluid samples was conducted to visualize the composition of the nanofluids and determine the particle size distribution and density variation within the test samples. The result from the particle size study conformed to the numerical model prediction for the sizes of the nanoparticle and the compressed layer—with the nanoparticulate entity possessing a dimension of 6.2 ± 0.6 nm. Thus, this study validates the implications of the nFE which accounts for the formation of a compressed layer within the nanofluid domain. The observed surplus density can definitely be attributed to the presence of the compressed layer having a thickness of ~2 nm. The current work is arguably the first reported study that has attempted to physically characterize (or confirm) the presence of compressed layer in oil-based nanofluids with the help of TEM imaging—a phenomenon hitherto suggested only by computational models. Densified hydrocarbons have significant potential for serving as radiation shields in deep space exploration vehicles. The results of the current study clearly demonstrate that the density of PCM oil (which is a hydrocarbon) can be significantly improved by introducing casein nanoparticles. In fact, the densities are in surplus of the prediction yielded by the traditional mixing rule for nanofluids. Hence, this study makes a strong case for the consideration of PCM oil-based nanofluids (with enhanced densities) as feasible candidates for space radiation shielding. Naturally, a progression of this research would involve evaluating the varying densities of distinct nanofluids comprising different combinations of solvents and nanoparticles.

Acknowledgment

Transmission electron microscopy and image analysis were performed at Texas A&M University's Microscopy and Imaging Center (RRID: SCR_022128). The use of the Texas A&M University Microscopy and Imaging Center Core Facility (RRID: SCR_022128) is acknowledged.

Conflict of Interest

There are no conflicts of interest. This article does not include research in which human participants were involved. Informed consent is not applicable. This article does not include any research in which animal participants were involved.

Data Availability Statement

The authors attest that all data for this study are included in the paper.

Nomenclature

m = mass, g
u = uncertainty
v = specific volume, cm^3/g or cc/g
x = mass fraction of nanoparticles in the nanofluid
y = mass fraction of compressed phase in the nanofluid
A = correction factor for oil-based nanofluids
B = correction factor for water-based nanofluids
V = volume, cm^3 or cc

Greek Symbols

δ = thickness of the compressed layer, nm
Δ = difference
ε = thickness of void region, nm
ρ = density, g/cc

Subscripts or Superscripts

a = air
c = compressed layer
f = base fluid
i = component reference
j = component reference
n = nanoparticle
$T1$ = accounting for the presence of nanoparticles and base fluid in the nanofluid medium
$T2$ = accounting for the presence of nanoparticles, compressed layer, and base fluid in the nanofluid medium
s = sinker
$stat$ = statistical
tf = test fluid
$V21$: = deviant specific volume
w = water
$a–w$ = difference in property value when measured in air and water.
$a–tf$ = difference in property value when measured in air and test fluid.

Acronyms and Abbreviations

ISS = International Space Station
LEO = low earth orbit
LNG = liquid natural gas
MD = molecular dynamic
NASA = National Aeronautics and Space Administration
nFE = nanofin effect
PCM = phase change material
TEM = transmission electronic microscopy

Table 10 Simple mixing rule prediction (considering contributions from milk protein, PCM oil, and NaOH)

Ingredient	Mass (g)	Mass fraction, x_i	Density ρ_i (g/cc)	$\frac{x_i}{\rho_i}$	$\sum \frac{x_i}{\rho_i}$	$\rho_{T1'}$ (g/cc)
PCM oil	40	0.980	0.86	1.14	1.165	0.86
NaOH	0.4	0.010	2.13	0.005		
Milk powder	0.4	0.010	0.5	0.02		

Appendix

In nature, milk protein does not inherently dissolve in PCM oil unless propelled by external surfactants/reactants (in this case, SDS, NaOH, and water).

Casein is essentially insoluble in neutral solvents such as de-ionized water and paraffin oil. The positively charged ions present in the structure neutralize the negative charges, rendering them insoluble when the pH of the medium is neutral [43,44]. However, if casein is introduced in a slightly acidic/basic solvent medium (prepared by introducing an acidic or basic entity in a neutral base solvent, as in the present study), ionization is induced in the acidic side chains (due to the formation of $-CO_2^-$) or basic side chains (due to the formation of the $-NH_3^+$) of the protein structure and makes it soluble in the medium.

SDS is a hydrophilic surfactant having a hydrophilic-lipophilic balance (HLB) value of 40 and it plays a pivotal role in forming the intermediate oil–water complex. Given its high HLB value, it is very unlikely that SDS will dissolve in oil. On the contrary, NaOH is known to react with oils during saponification reactions.

Therefore, accounting for the presence of NaOH in the fluid medium may help in deriving a more realistic estimation of the test fluid density. Table 10 lists the density (ρ_{T1}) estimation of the test fluid considering that the oil-dominant fluid layer contains PCM oil, milk protein, and NaOH.

The relative difference between ρ_{T1} and ρ_{T1} (stated in Table 2) is 1.17% and it is within the measurement uncertainty range of our experimental apparatus (which will be discussed in the subsequent section) and hence is unlikely to be a cause of concern in the numerical analyses and discussions presented hereafter. Therefore, the effective oleo-nanofluid density prediction, ρ_{T1}, as listed in Table 2, will serve as the baseline simple mixing rule estimate for comparison with experimentally measured nanofluid densities.

References

[1] Ma, B., Kumar, N., and Kuchibhotla, A., 2018, "Experimental Measurement of the Effect of Particle Concentration on the Specific Heat Capacity of Silica Nanofluids," 2018 17th IEEE Intersociety Conference on Thermal and Thermomechanical Phenomena in Electronic Systems (ITherm), San Diego, CA, May 29–June 1, pp. 246–251.

[2] Jo, B., and Banerjee, D., 2011, "Interfacial Thermal Resistance Between a Carbon Nanoparticle and Molten Salt Eutectic: Effect of Material Properties, Particle Shapes and Sizes," ASME/JSME Thermal Engineering Joint Conference, Honolulu, HI, Mar. 13–17, Vol. 38921, p. 7.

[3] Lee, J., Kuchibhotla, A., Banerjee, D., and Berman, D., 2019, "Silica Nanoparticles as Copper Corrosion Inhibitors," Mater. Res. Expr., **6**(8), p. 0850e3.

[4] Kuchibhotla, A., Chakraborty, S., and Banerjee, D., 2020, "Experimental Validation of Numerical Predictions for "Deviant" Density Enhancement of Protein Emulsions in Oil (Oleo-Nanofluids)," SN Appl. Sci., **2**(1617), pp. 1–13.

[5] Oh, S. H., Kauffmann, Y., Scheu, C., Kaplan, W. D., and Rühle, M., 2005, "Ordered Liquid Aluminum at the Interface With Sapphire," Science, **310**(5748), pp. 661–663.

[6] Huisman, W. J., Peters, J. F., Derks, J. W., Ficke, H. G., Abernathy, D. L., and van der Veen, J. F., 1997, "A New X-ray Diffraction Method for Structural Investigations of Solid-Liquid Interfaces," Rev. Sci. Instrum., **68**(11), pp. 4169–4176.

[7] Jo, B., 2012, "Numerical and Experimental Investigation of Organic Nanomaterials for Thermal Energy Storage and for Concentrating Solar Power Applications," Ph.D. dissertation, Texas A&M University, College Station, TX.

[8] Shin, D., and Banerjee, D., 2015, "Enhanced Thermal Properties of SiO_2 Nanocomposite for Solar Thermal Energy Storage Applications," Int. J. Heat Mass Transfer, **84**, pp. 898–902.

[9] Shin, D., and Banerjee, D., 2010, "Enhanced Specific Heat of Silica Nanofluid," ASME J. Heat Transfer-Trans. ASME, **133**(2), p. 024501.

[10] Tiznobaik, H., Banerjee, D., and Shin, D., 2015, "Effect of Formation of "Long Range" Secondary Dendritic Nanostructures in Molten Salt Nanofluids on the Values of Specific Heat Capacity," Int. J. Heat Mass Transfer, **91**, pp. 342–346.

[11] Ma, B., and Banerjee, D., 2019, "Numerical Modeling of Nanofluid Thermal Conductivity: The Effect of Nanonetwork on Thermal Transport Behavior," ASME J. Heat Transfer-Trans. ASME, **141**(12), pp. 122401.

[12] Singh, N., and Banerjee, D., 2014, *Nanofins: Science and Applications*, Springer, New York.

[13] Sathyamurthi, V., Ahn, H. S., and Banerjee, D., 2009, "Subcooled Pool Boiling Experiments on Horizontal Heaters Coated with Carbon Nanotubes," ASME J. Heat Mass Transfer-Trans. ASME, **131**(7), p. 071501.

[14] Zhong, H., and Lukes, J. R., 2006, "Interfacial Thermal Resistance Between Carbon Nanotubes: Molecular Dynamics Simulations and Analytical Thermal Modeling," Phys. Rev. B, **74**(12), pp. 125403.

[15] Estrada, D., and Pop, E., 2011, "Imaging Dissipation and Hot Spots in Carbon Nanotube Network Transistors," Appl. Phys. Lett., **98**(7), p. 073102.

[16] Pollack, G. L., 1969, "Kapitza Resistance," Rev. Mod. Phys., **41**(1), pp. 48–81.

[17] Singh, N., 2010, "Computational Analysis of Thermo-Fluidic Characteristics of a Carbon Nano-Fin," Ph.D. dissertation, Texas A&M University, College Station, TX.

[18] Maune, H., Chiu, H., and Bockrath, M., 2006, "Thermal Resistance of the Nanoscale Constrictions Between Carbon Nanotubes and Solid Substrates," Appl. Phys. Lett., **89**(1), p. 013109.

[19] Murad, S., and Puri, I. K., 2008, "Thermal Transport Across Nanoscale Solid-Fluid Interfaces," Appl. Phys. Lett., **92**(13), p. 133105.

[20] Huxtable, S. T., Cahill, D. G., Shenogin, S., Xue, L., Ozisik, R., Barone, P., Usrey, M., et al., 2003, "Interfacial Heat Flow in Carbon Nanotube Suspensions," Nat. Mater., **2**(11), pp. 731–734.

[21] Jung, S., 2012, "Numerical and Experimental Investigation of Inorganic Nanomaterials for Thermal Energy Storage (TES) and Concentrated Solar Power (CSP) Applications," Ph.D. dissertation, Texas A&M University, College Station, TX.

[22] Shin, D., 2011, "Molten Salt Nanomaterials for Thermal Energy Storage and Concentrated Solar Power Applications," Ph.D. dissertation, Texas A&M University, College Station, TX.

[23] Yang, H., 2014, "Experimental and Numerical Investigation of Pool Boiling Heat Transfer on Engineered Nano-Finned Surfaces," Ph.D. dissertation, Texas A&M University, College Station, TX.

[24] Li, L., Zhang, Y., Ma, H., and Yang, M., 2010, "Molecular Dynamics Simulation of Effect of Liquid Layering Around the Nanoparticle on the Enhanced Thermal Conductivity of Nanofluids," J. Nanopart. Res., **12**(3), pp. 811–821.

[25] Chang, C.-I., Lee, W.-J., Young, T.-F., Ju, S.-P., Chang, C.-W., Chen, H.-L., and Chang, J.-G., 2008, "Adsorption Mechanism of Water Molecules Surrounding Au Nanoparticles of Different Sizes," J. Chem. Phys., **128**(15), p. 154703.

[26] Jo, B., and Banerjee, D., 2015, "Effect of Solvent on Specific Heat Capacity Enhancement of Binary Molten Salt-Based Carbon Nanotube Nanomaterials for Thermal Energy Storage," Int. J. Therm. Sci., **98**, pp. 219–227.

[27] Vajjha, R. S., Das, D. K., and Mahagaonkar, B. M., 2009, "Density Measurement of Different Nanofluids and Their Comparison With Theory," Pet. Sci. Technol., **27**(6), pp. 612–624.

[28] Mariano, A., Pastoriza-Gallego, M. J., Lugo, L., Camacho, A., Canzonieri, S., and Piñeiro, M. M., 2013, "Thermal Conductivity, Rheological Behaviour and Density of Non-Newtonian Ethylene Glycol-Based SnO_2 Nanofluids," Fluid Phase Equilib., **337**, pp. 119–124.

[29] Pastoriza-Gallego, M. J., Casanova, C., Páramo, R., Barbés, B., Legido, J. L., and Piñeiro, M. M., 2009, "A Study on Stability and Thermophysical Properties (Density and Viscosity) of Al_2O_3 in Water Nanofluid," J. Appl. Phys., **106**(6), p. 064301.

[30] Heyhat, M. M., Kowsary, F., Rashidi, A. M., Momenpour, M. H., and Amrollahi, A., 2013, "Experimental Investigation of Laminar Convective Heat Transfer and Pressure Drop of Water-Based Al_2O_3 Nanofluids in Fully Developed Flow Regime," Exp. Therm. Fluid. Sci., **44**, pp. 483–489.

[31] Selvakumar, R. D., and Wu, J., 2019, "A Comprehensive Model for Effective Density of Nanofluids Based on Particle Clustering and Interfacial Layer Formation," J. Mol. Liq., **292**, p. 111415.

[32] Sharifpur, M., Yousefi, S., and Meyer, J. P., 2016, "A New Model for Density of Nanofluids Including Nanolayer," Int. Commun. Heat Mass Transfer, **78**, pp. 168–174.

[33] Yu, C., Richter, A. G., Datta, A., Durbin, M. K., and Dutta, P., 1999, "Observation of Molecular Layering in Thin Liquid Films Using X-ray Reflectivity," Phys. Rev. Lett., **82**(11), pp. 2326–2329.

[34] Yu, C.-J., Richter, A. G., Kmetko, J., Dugan, S. W., Datta, A., and Dutta, P., 2001, "Structure of Interfacial Liquids: X-ray Scattering Studies," Phys. Rev. E, **63**(2), p. 021205.

[35] Rask, J., Vercoutere, W., and Navarro, B. J., 2008, *Space Faring: The Radiation Challenge*, National Aeronautics and Space Administration. https://www.nasa.gov/wpcontent/uploads/2009/07/284273main_radiation_hs_mod1.pdf
[36] "Comprehensive Guide on Polyethylene (PE)," https://omnexus.specialchem.com/selection-guide/polyethylene-plastic. Accessed April 14, 2024.
[37] Narici, L., Casolino, M., Di Fino, L., Larosa, M., Picozza, P., Rizzo, A., Zaconte, V., 2017, "Performances of Kevlar and Polyethylene as Radiation Shielding On-Board the International Space Station in High Latitude Radiation Environment," Sci. Rep., **7**(1), pp. 1644.
[38] Singleterry, R. C., 2013, "Radiation Engineering Analysis of Shielding Materials to Assess Their Ability to Protect Astronauts in Deep Space From Energetic Particle Radiation," Acta Astronaut., **91**, pp. 49–54.
[39] Choi, S., and Eastman, J. A., 1995, "Enhancing Thermal Conductivity of Fluids With Nanoparticles," International Mechanical Engineering Congress and Exhibition, San Francisco, CA, Nov. 12–17.
[40] Feibelman, P. J., 2010, "The First Wetting Layer on a Solid," Phys. Today, **63**(2), pp. 34–39.
[41] Davey, R., "Silicon Dioxide Nanoparticles (Nanosilica): Properties & Applications," https://www.azonano.com/article.aspx?ArticleID=3398. Accessed April 14, 2024.
[42] Pugliese, A., Cabassi, G., Chiavaro, E., Paciulli, M., Carini, E., and Mucchetti, G., 2017, "Physical Characterization of Whole and Skim Dried Milk Powders," J. Food Sci. Technol., **54**(11), pp. 3433–3442.
[43] "What If It's an Acid and a Base?," https://www.flinnsci.ca/api/library/Download/272d39f05bb14b689cacbc91cb463573. Accessed April 14, 2024.
[44] Newman, L. M., 2018, "Milk Casein Proteins: Ancient, Diverse, and Essential," International Milk Genomics Consortium. https://www.milkgenomics.org/?splash=milk-casein-proteins-ancient-diverse-essential. Accessed April 14, 2024
[45] "Sodium Hydroxide Pellets SDS," https://www.emdmillipore.com/US/en/product/msds/MDA_CHEM-106482. Accessed April 14, 2024.
[46] Dinçer, İ, and Zamfirescu, C., 2015, *Drying Phenomena: Theory and Applications*, John Wiley & Sons, New York, pp. 457–459.
[47] Heymann, J. B., 2018, "Guidelines for Using Bsoft for High Resolution Reconstruction and Validation of Biomolecular Structures From Electron Micrographs," Protein Sci., **27**(1), pp. 159–171.
[48] Abràmoff, M. D., Magalhães, P. J., and Ram, S. J., 2004, "Image Processing With ImageJ," Biophotonics Int., **11**(7), pp. 36–42.
[49] "PureTemp 15 Technical Information," https://puretemp.com/wp-content/uploads/2021/06/PureTemp15TechnicalDataSheet.pdf, Accessed April 14, 2024.